Carbohydrate Polymers 343 (2024) 122473

Contents lists available at ScienceDirect

Carbohydrate Polymers

journal homepage: www.elsevier.com/locate/carbpol

Highly branched thermoresponsive polysaccharide derivative in water. Partly substituted highly branched cyclic dextrin ethylcarbamate

Akihito Kobayashi, Ken Terao *

Department of Macromolecular Science, Graduate School of Science, Osaka University, 1-1 Machikaneyama-cho, Toyonaka, Osaka 560-0043, Japan

ARTICLE INFO

Keywords:
Water soluble polysaccharide derivative
Highly branched polysaccharide
LCST
Small-angle X-ray scattering
Inclusion complex

ABSTRACT

A thermoresponsive highly branched polysaccharide derivative was revealed from commercially available highly branched cyclic dextrin (HBCD), originally synthesized from amylopectin. Eight samples of partially substituted ethyl carbamate derivatives of HBCD (HEC) were prepared with a degree of substitution DS ranging from 0.27 to 1.46. Three samples with DS = 0.88, 1.05, and 1.22 showed LCST type phase separation in water. The intrinsic viscosity and form factor in water were typical of the hyperbranched structure. The intermolecular interactions between HEC and iodine or 1-anilinonaphthalene-8-sulfonic acid (ANS) were appreciably different from those of the linear analog (AEC), suggesting that the locally bent helical conformation of highly branched HEC chains has a different interaction with small molecules. The phase diagram of HEC-water systems was accidentally similar to that of the linear chain with the same molar mass and DS, although the one phase region of the branched polymer chain-poor solvent system is usually wider than that of the corresponding linear chain. This is likely due to the lower hydration nature of the polymer segment of HEC chains than that of the corresponding linear chain.

1. Introduction

Macromolecules tend to be less soluble in many solvents due to the low entropy gain on dissolution. Since the solvation affinity can be controlled by chemical modification of polysaccharides, phase separation behavior is also found for polysaccharide derivatives (Burchard, 1969). For aqueous systems, cellulose ethers are widely used for versatile applications, while they mainly exhibit LCST (lower critical solution temperature) type phase separation behavior (Bizmark et al., 2022; Chevillard & Axelos, 1997; Heymann, 1935; McAllister et al., 2015; Nishida et al., 2017; Sarkar, 1979). Aqueous phase separation behavior has also been found for the other polysaccharides, i.e., dextran (Otto et al., 2021), chitosan (Chen et al., 2022), starch (Jong & Ju, 2017; Ju et al., 2012; Ju et al., 2013; Yuan et al., 2014; Zheng et al., 2019), xylan (Gericke et al., 2024), and amylose (Kimura et al., 2020; Nakata et al., 2024). The LCST type phase separation is related to the temperature dependent hydration-dehydration behavior. Thus, the polymer-solvent interactions play an important role in the phase separation. Among them, the nonlinear polysaccharide derivative with thermoresponsive behavior is limited to starch derivatives (Jong & Ju, 2017; Ju et al., 2012; Ju et al., 2013; Yuan et al., 2014; Zheng et al., 2019). However, the data for starch derivatives cannot be used to discuss the branching effect on phase separation because that of the corresponding linear chain has not been reported.

In general, nonlinear polymers have better solubility than the corresponding linear polymers of the same molar mass. In fact, much work has been done on synthetic branched polymers, i.e., star branched (Alessi et al., 2004; Cowie et al., 1979; Tasaka et al., 2008; Terao et al., 1998; Yokoyama et al., 1991), randomly branched (S. Sato et al., 1985), and ring polymers (Jung et al., 2017; Qiu et al., 2007), while it cannot be easily explained in terms of the classical mean-field approximation theory, and some recent calculations can predict the difference of the phase diagram of linear and nonlinear polymers in solution (Browarzik et al., 2013; Yang et al., 2006). Recently, it has been reported that hyperbranched poly(*N*-isopropyl acrylamide) has a lower LCST than that of the linear polymer (Kojima et al., 2022). This phenomenon has been explained in terms of cooperative hydration. On the other hand, we have recently shown that both cyclic and hyperbranched amylose carbamate derivatives have significantly different interactions with small molecules based on the chiral recognition ability (Kishimoto et al., 2022; Kishimoto et al., 2023; Ryoki et al., 2019), the second virial coefficient (Asano et al., 2013), and the phase separation behavior in organic solvents (Mizuguchi et al., 2023). This is because the local curvature of the polymer chains is affected by the cyclic or highly

* Corresponding author.
E-mail address: terao.ken.sci@osaka-u.ac.jp (K. Terao).

https://doi.org/10.1016/j.carbpol.2024.122473
Received 9 May 2024; Received in revised form 6 July 2024; Accepted 8 July 2024
Available online 9 July 2024

branched structures.

We recently found that a linear polysaccharide derivative, partially substituted linear amylose ethylcarbamate, is soluble in water and the LCST-type phase separation behavior was observed (Kimura et al., 2020). Consequently, the partially substituted ethylcarbamate derivative (HEC) of highly branched cyclic dextrin (HBCD), which is enzymatically produced from amylopectin, may be a good model branched polysaccharide with thermoresponsive nature due to its relatively narrow molar mass dispersity. The phase diagram of HEC-water systems as well as the interaction with small molecules were investigated by phase separation experiments, absorption, and fluorescence spectra. Another characteristic feature of highly branched polymers is a much lower solution viscosity due to their significantly more compact dimensions in solution than the corresponding linear polymers. To confirm this, the intrinsic viscosity and form factor were also estimated from viscosity and small-angle X-ray scattering measurements, respectively, to compare the dimensional properties with the corresponding linear chain.

2. Experimental section

2.1. Samples

A reagent grade highly branched cyclic dextrin (HBCD) sample (Fujifilm Wako) was used as the source of branched polysaccharide for the synthesis of HEC. The average repeat unit of α-1,6-linkage hydrolyzed HBCD was estimated to be 16 (Takata et al., 1996; Takata et al., 2003). It can be confirmed by ^{1}H NMR measurement in D_2O at 80 °C referring to the literature for amylopectin (Nilsson et al., 1996) (Fig. S1). The synthesis procedure was substantially the same as that of the previously reported amylose ethylcarbamate (AEC) (Kimura et al., 2020). A typical procedure for evaluating **HEC300K1.22** is as follows. 3.1 g (19 mmol in the repeat unit) of the HBCD sample and LiCl (3 g) were dried in a vacuum in a two-necked flask at 90 °C for 3 h. *N*,*N*-dimethylacetamide (80 mL) was added to the flask under an Ar atmosphere. After stirring at 90 °C to completely dissolve the solid sample, dry pyridine (80 mL) and ethyl isocyanate (2.0 mL, 26 mmol) were added to the HBCD solution. The resulting mixture was stirred at 90 °C for at least 1 d. The crude polymer sample was purified by reprecipitation in acetone. A 7.2 g powdered sample was obtained. The sample was dissolved in 350 mL of water and dialyzed in pure water at 3 °C for at least 4 d using a SPECTRA/POR regenerated cellulose membrane with a MWCO of 12,000–14,000. The resulting aqueous solution was evaporated to 30 mL and lyophilized to obtain a white solid HEC sample. The other samples were prepared in the same manner with different amounts of ethyl isocyanate. Water-insoluble samples were purified by reprecipitation with methanol as solvent and methyl acetate as precipitant. We also prepared some linear AEC samples from enzymatically synthesized amylose to obtain linear AEC samples with molar masses relatively close to the current HEC samples. The HEC and AEC samples used in this study are summarized in Table 1. All samples were characterized by ^{1}H NMR in DMSO-d_6 and ATR-FTIR. Some example spectra are shown in Figs. S2 and S3; note that the NMR spectrum at 90 °C was substantially similar to that at 25 °C. The ^{13}C NMR spectra for **HEC300K1.22** in DMSO-d_6 at 90 °C (Fig. S4) indicate that no specific regioselectivity was found. The ultimate analysis was made for all samples to determine the weight fractions of carbon and nitrogen. The C/N weight ratio gives the degree of substitution DS, where DS = 3 for complete substitution. The evaluated DS values are summarized in Table 1.

2.2. Characterization of HEC and AEC in dilute organic solvent

Since the solubility in water for both HEC and AEC depends significantly on DS as summarized in Table 1, the molar mass values of the samples were determined in dimethylformamide (DMF).

Conventional static light scattering measurements were made for **HEC200K0.27**, **HEC220K0.55**, and **HEC170K0.75** in DMF at 25 °C using an ALV/SLS/DLS-5000 light scattering photometer. The incident light source was an Nd:YAG laser with a wavelength of $\lambda_0 = 532$ nm in a vacuum. Each solution and the solvent were optically cleaned through a 0.22 μm PTFE membrane filter. The refractive index increment $\partial n/\partial c$, the mandatory constant for evaluating the molar mass from the scattering intensity, was determined for each sample in DMF at 25 °C using a modified Schultz-Cantow type differential refractometer (Shimazu Co., Japan). The resulting Rayleigh ratio R_θ (the absolute scattering intensity) at different polymer mass concentrations c and the magnitude q of the scattering vector were analyzed in terms of the Guinier plot, as shown in Fig. S5, to determine the weight-average molar mass M_w, for which the experimental error is estimated to be ±15 % based on the variability of the data. Notably, the radius of gyration was not estimated from the current data due to the very weak q dependence of R_θ, i.e. the gyration radii are shown to be less than 20 nm.

Size-exclusion chromatography (SEC) equipped with multi-angle light scattering (MALS) and concentration detectors was performed on the HEC and AEC samples to determine M_w. SEC-MALS measurements were examined for the samples in THF to determine the weight-average molar mass M_w and molar mass dispersity using a DAWN DSP MALS photometer (Wyatt) and a RI-4030 refractive index detector (Jasco). A Shodex guard column Asahipak GF-1G 7B and a Shodex SEC column Asahipak GF-7 M HQ were connected in series and installed in a column

Table 1
Molecular characteristics of HEC (branched) and AEC (linear) samples.

Sample	Yield /%	DS [a]	M_w / kg mol^{-1}	n_w	[η] / cm^{3}g^{-1}	Solubility in water
HEC200K0.27	82	0.27	200 [b] (195[c])	1100	17.2[d]	S
HEC220K0.55	70	0.55	220 [b] (193[c])	1100	17.1[d]	S
HEC170K0.75	83	0.75	170 [b] (164[c])	770	15.4[d]	S
HEC190K0.88	72	0.88	190 [b]	850	–	P
HEC230K1.05	66	1.05	230 [b]	970	16.7[e]	P
HEC300K1.22	78	1.22	300 [b]	1200	–	P
HEC1.43	72	1.43	–	–	–	I
HEC1.46	62	1.46	–	–	–	I
AEC160K0.44	83	0.44	160 [b]	830	34.0[d]	S
AEC200K0.64	73	0.64	200 [b]	970	48.1[d]	S
AEC130K0.95	–	0.95	190 [b]	570	40.5[e]	P
AEC220K1.18	46	1.18	130 [b]	900	–	P

I: insoluble. S: soluble between 4 and 80 °C. P: phase separation was observed.
[a] DS = 3 for full substitution.
[b] From SEC-MALS in DMF.
[c] From SLS in DMF.
[d] In water at 25 °C.
[e] In water at 0.3°C.

oven at 40 °C with a flow rate of 0.5 mL min^{-1}. Two polystyrene standards (Tosoh TSKgel Standard PS F-4, M_w = 37.9 kg mol^{-1} and F-40, M_w = 427 kg mol^{-1}) were used to calibrate both the MALS and RI detectors. For the HEC samples, the double peak was evaluated as shown in Fig. S6. Since the M_w value calculated from the second peak is substantially the same as that from the conventional light scattering described above, the first peak is due to aggregation of the sample. Possible reasons are higher column temperature or high share rate in the SEC column or tubing. We therefore estimated the M_w value from the second peak. The resulting M_w values are summarized in Table 1. Although essentially the same chromatogram was observed from multiple measurements, the experimental error can be estimated to be approximately ±15 % due to the above-mentioned significant aggregation. The weight-average number n_w of AGU units in a molecule calculated from M_w and DS ranges between 800 and 1200. These values are close to or slightly lower than those for completely substituted phenylcarbamate (Mizuguchi et al., 2023) and 3,5-dimethylphenylcarbamate (Kishimoto et al., 2022) derivatives synthesized from the same HBCD sample.

2.3. Small-angle X-ray scattering (SAXS)

SAXS measurements were made for **HEC200K0.27** and **HEC170K0.75** in water at 20 °C at the BL40B2 beamline in SPring-8 (Hyogo, Japan). The solvent water or the polymer solutions with three different c ranging from 2 to 11 mg mL^{-1} were filled into a specially designed cell in which a 2 mmϕ quartz capillary is fixed, in order to properly subtract the scattering intensity of the solvent from that of the solution. The X-ray energy was chosen to be 12 keV (λ_0 = 0.1 nm) and the intensity was detected both upstream and downstream of the solution cell to compensate for the intensity fluctuation and transmission of the X-ray. The scattered X-ray was detected using a Dectris Pilatus 3 2 M photon counting equipment located 4.2 m downstream of the sample position. The magnitude q of the scattering vector at each pixel on the detector was determined from the diffraction pattern of silver behenate.

2.4. Viscometry

Although scattering measurements are difficult for partially substituted carbamate derivatives of linear and branched ethylcarbamate derivatives due to the small amount of large aggregates, viscosity measurements provide reliable information on polymer dimensions. Viscosity measurements for HEC and AEC samples in dilute aqueous solution were examined using a custom-made conventional Ubbelohde type viscometer, for which the minimum required solution is 3 mL and the water flow rate is approximately 150 s. At least three flow-time measurements were made for each solvent and solution to confirm repeatability of less than 1 % in specific viscosity. The evaluated specific viscosity for three or four different c ranging from c = 5 to 30 mg mL^{-1} was analyzed using the Huggins and Mead-Fuoss plots to evaluate the intrinsic viscosity [η].

2.5. Phase separation experiments

Because HEC and AEC samples with intermediate DS dissolve in water and the solution exhibits phase separation behavior with increasing temperature, turbidity measurements were performed on the HEC and AEC samples in water using a Jasco V-550 or V-750 spectrometer (Jasco Co., Japan). A rectangular quartz cell with a path length of 2 mm was placed in a thermostatic cell holder that was heated at a constant rate of 0.5 or 1 K/min. Optical transmittance was detected at λ_0 = 550 or 800 nm, depending on the absorption of added small molecules, as described below. The repeatability of the data was verified by measuring many polymer solutions at different concentrations.

2.6. Spectroscopy in the presence of small molecules

A small amount of I_2-KI aqueous solution (50 mM) was added to a HEC or AEC solution (1.5 mL) with c of 5 mg mL^{-1} to prepare the test solution with an I_2 concentration of 0.3 mM. The UV–vis absorption spectra of the solution filled in a 2 mm path length rectangular quartz cell were evaluated using a Jasco V-550 or V-750 spectrometer (Jasco Co., Japan) at different temperatures.

An appropriate amount of HEC or AEC sample was added to 0.1 mM 1-anilinonaphthalene-8-sulfonic acid (ANS) aqueous solution to prepare the solution with a polymer mass concentration c of 30 mg mL^{-1}. The resulting solution was filtered through a 0.8 μm cellulose acetate filter. Dry nitrogen was brown in the solution immediately before measurement. A Hitachi F-4500 or Shimazu RF-5300PC fluorescence spectrophotometer was used to determine the fluorescence spectra at the excitation wavelength of 355 nm at different temperatures between 10 and 70 °C.

Similar fluorescence measurements were made for HEC or AEC with pyrene in aqueous solution at 26 °C at the excitation wavelength of 337 nm. The solution was prepared by adding a small amount of a saturated methanol solution of pyrene. The pyrene concentration was estimated from the absorbance of the solution at λ_0 = 338 nm. We have verified repeatability by multiple measurements at least twice for all spectroscopic measurements described in this section.

3. Results and discussion

3.1. Dimensional and hydrodynamic properties in water

To estimate the molecular structure of HEC samples with high solubility in water, SAXS measurements were examined for aqueous solutions of **HEC200K0.27** and **HEC170K0.75**. The excess scattering intensity $\Delta I(q)$ is substantially proportional to c in the entire q range investigated, indicating that the molecular structure and dispersion state do not depend on the c range. This result also confirms the repeatability of the SAXS measurements. We therefore estimated the form factor $P(q)$ from $\Delta I(q)$ using the Guinier plot. The resulting $P(q)$ data are plotted against q in Fig. 1, where the repeatability estimated from the concentration variations of $\Delta I(q)/c$ is comparable to the size of the circles. The steep reduction with a slope of −2.7 is typical for highly branched macromolecules (Lederer & Burchard, 2015). The $P(q)$ data were analyzed in terms of the theory for hyperbranched polymers (Burchard, 2004), which can adequately explain $P(q)$ for completely substituted HBCD carbamate derivatives (Kishimoto et al., 2022; Mizuguchi et al., 2023). The form factor $P(q)$ is written as

$$P(u)=\left[\frac{sin[(d-1)arctan(\zeta_{br}u)]}{(d-1)(\zeta_{br}u)(1+{\zeta_{br}}^2u^2)^{(d-1)/2}}\right]^2 \Bigg/ \left[\frac{sin[(d-1)arctan(\zeta_{lin}u)]}{(d-1)(\zeta_{lin}u)(1+{\zeta_{lin}}^2u^2)^{(d-1)/2}}\right] \quad (1)$$

with

$${\zeta_{br}}^2=\frac{C+1}{d(d+1)} \quad (2)$$

$${\zeta_{lin}}^2=\frac{2C}{d(d+1)} \quad (3)$$

where $1/C$, d, and u denote the number of branching points, the fractal dimension of the partial chains, and the reduced scattering vector defined as $u = q R_g$, where R_g is the radius of gyration of the hyperbranched chain. When $1/C$ is estimated from both n_w and the ratio of α-1,6 to α-1,4 linkages determined from ^{1}H NMR of HBCD shown in Fig. S1, R_g and d are the resulting fitting parameters. The two parameters are chosen to be R_g = 11.8 nm and d = 1.90 for **HEC200K0.27** ($1/C$ =

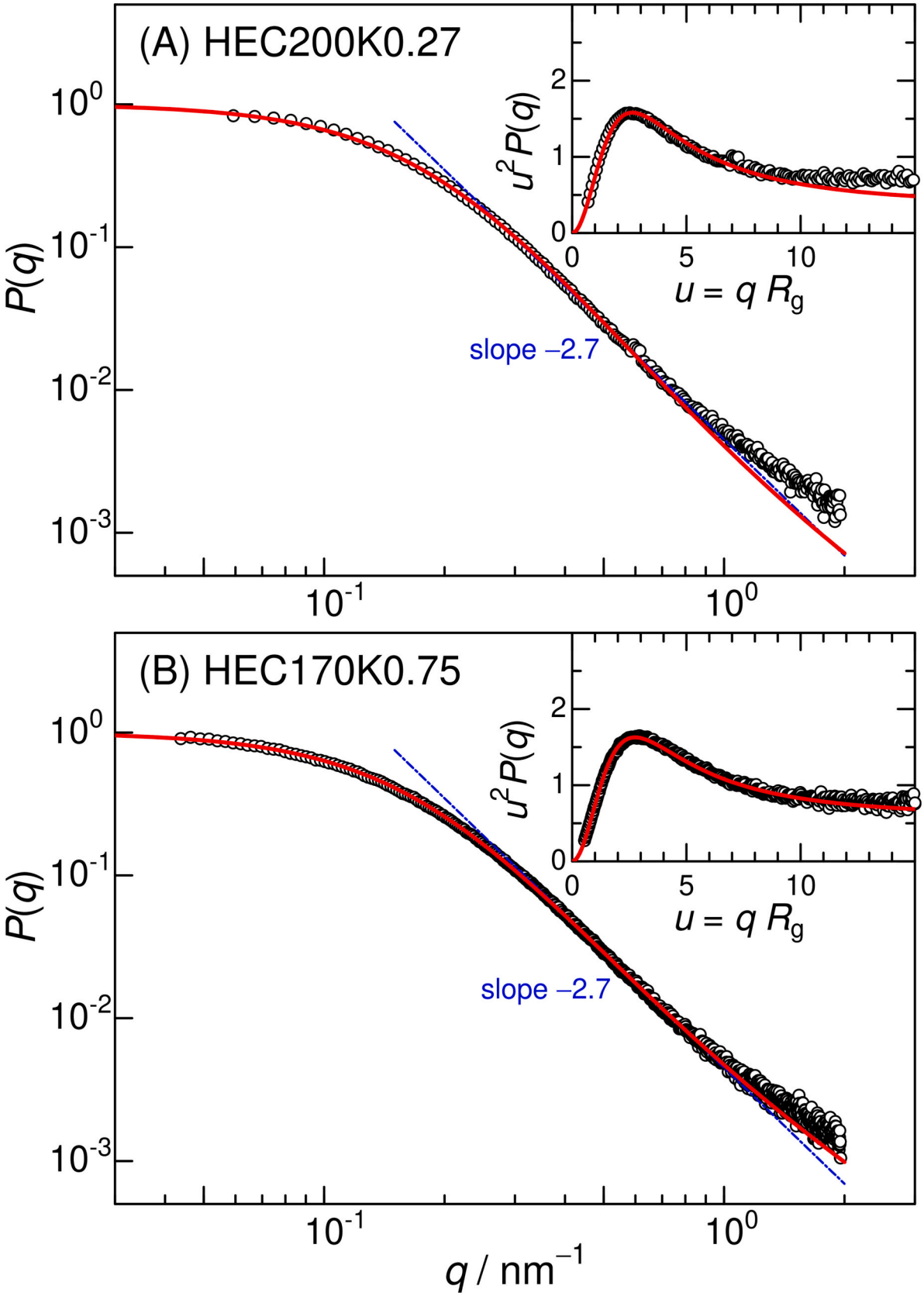

Fig. 1. Double logarithmic plots of the form factor $P(q)$ vs. q for (A) **HEC200K0.27** and (B) **HEC170K0.75** in water at 20 °C. The inset of each panel is the Kratky plot. Solid red curves denote the theoretical values from eq. 1. (For interpretation of the references to colour in this figure legend, the reader is referred to the web version of this article.)

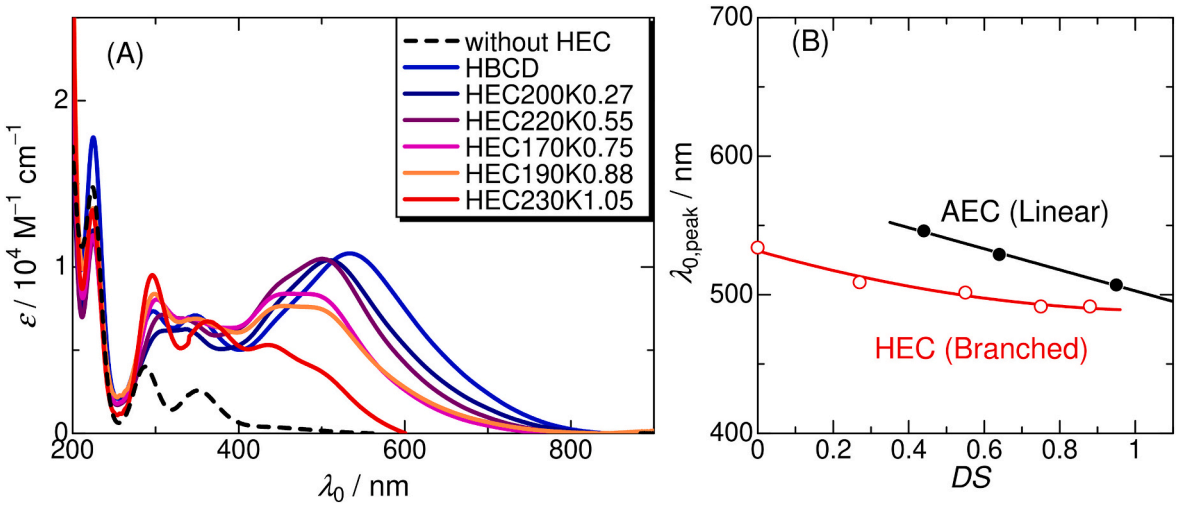

Fig. 2. (A) UV–vis absorption spectra for the HEC samples with aqueous KI–I_2 solution at 20 °C. Dashed curve is the data without HEC. The polymer mass concentration of AEC was 5 mg mL^{-1}, and the molar concentration of both I2 and KI are 50 mM. (B) DS dependence of the peak wavelength λ_0, peak for HEC along with the data for linear (AEC) samples.

55) and $R_g = 12.5$ nm and $d = 1.85$ for **HEC170K0.75** ($1/C = 39$). These parameters are consistent with our recent research (Kishimoto et al., 2022; Mizuguchi et al., 2023) and suggest the hyperbranched structure of HEC samples. Considering that the possible d range is from 1.7 (good solvent limit) to 2.0 (theta solvent), the current d values suggest that water has an intermediate solvent quality for water-soluble HEC samples. The compact dimensions of HEC are also confirmed by the intrinsic viscosity data summarized in Table 1, where the $[\eta]$ values for HEC samples are systematically smaller than those for linear AEC with similar M_w.

3.2. Complex formation with small molecules in water

To reveal the polymeric branching effects on the intermolecular interaction with small molecules, the complex formation behavior of HEC with iodine, ANS, and pyrene in aqueous solution was investigated. Fig. 2(A) shows the absorption spectra for aqueous KI–I_2 solution in the absence or presence of HEC. The significant absorption in the visible light wavelength range clearly indicates the complex formation of HEC and iodine. The peak wavelength $\lambda_{0,peak}$ plotted against DS in Fig. 2(B) is systematically smaller than that for the corresponding linear AEC. It should be noted that the data points for the linear polymer were determined for the current AEC samples listed in Table 1. This is most likely due to the short partial chains of HEC, considering the absorption behavior of amylose and amylopectin containing I_2. Another important point is that the $\lambda_{0,peak}$ of HEC decreases with increasing DS, but the difference between branched and linear chains becomes smaller. This is because the ethylcarbamate groups inhibit complexation and the absorption behavior becomes closer to that of the short amylose chains. Similar peak shifts between HEC and AEC also suggest the random substitution of ethylcarbamate groups. The complexation of HEC becomes less significant with increasing temperature, as is the case for linear AEC, as illustrated in Fig. S7, suggesting that the binding energy is essentially comparable to RT at room temperature, where R and T are the gas constant and absolute temperature, respectively. This is consistent with the previous report for amylose (Knutson et al., 1982).

Since ANS has a significant environment-dependent peak shift in the fluorescence spectrum (Klymchenko & Mely, 2013), the complex formation ability with ANS was also confirmed by the fluorescence spectra shown in Fig. 3(A), where the high fluorescence is found only for the spectra in the presence of HEC. Fig. 3(B) and Fig. 3(C) show the DS dependence of the peak wavelength $\lambda_{0,peak}$ and intensity I_{peak},

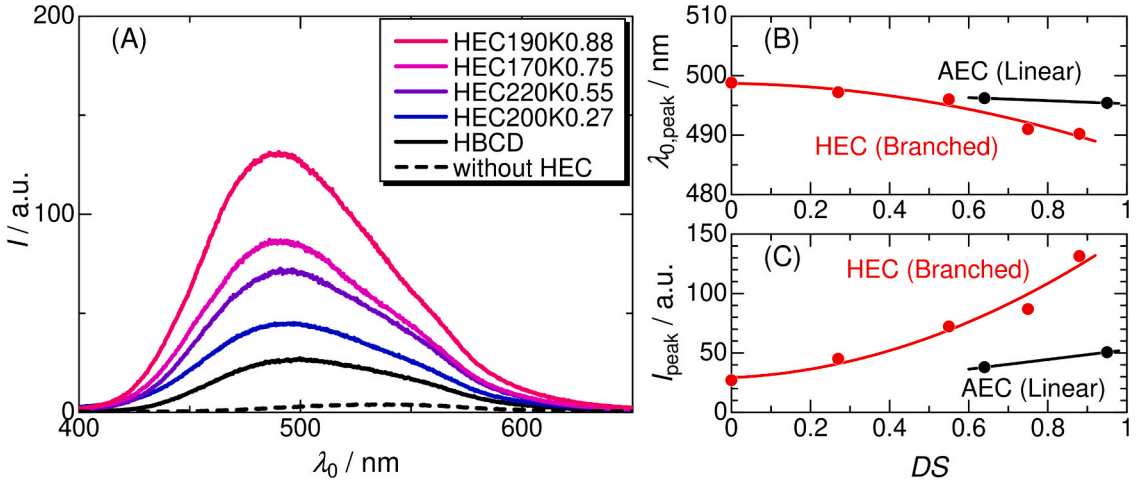

Fig. 3. Fluorescence spectra of 1-anilinonaphthalene-8-sulfonic acid (ANS) with the indicated HEC samples in water at 20 °C. Dashed curve is the data without HEC. The polymer mass concentration of AEC was 30 mg mL^{-1}, and the molar concentration of ANS is 0.1 mM. (B) DS dependence of the peak wavelength $\lambda_{0,peak}$ for HEC and AEC in water at 20 °C. (C) DS dependence of the peak intensity $I_{0,peak}$ for HEC and AEC in water at 20 °C.

respectively. The latter I_{peak} value increases significantly with increasing DS, indicating the hydrophobic nature of the ethylcarbamate groups. Furthermore, the value is significantly larger than that of the linear chain at the same DS, suggesting a more hydrophobic environment of HEC than that of AEC. This is most likely because the bent conformation around the branching points exhibits the hydrophobic nature. This seems to be related to our recent finding for specific LCST-type phase behavior of highly branched phenylcarbamate of HBCD (Mizuguchi et al., 2023) where no phase separation was observed for the corresponding linear chains in the same solvent condition. The specific chiral separation ability of HBCD-based chiral stationary phases may also be related to the bent conformation effect (Kishimoto et al., 2022). The temperature dependence shown in Fig. S8 is normal in that the I_{peak} decreases significantly with increasing temperature for both branched and linear chains. Specific fluorescence behavior was also found for the HEC-pyrene complex, as shown in Fig. S9, where a significant fluorescence peak for the excimer is found around $\lambda_0 = 430$ nm, especially for **HEC170K0.75**, indicating a hydrophobic environment in the HEC molecules as in the case of polysaccharide based polymer micelles (Sato et al., 2022).

3.3. Phase separation behavior of aqueous AEC solutions

As shown in Table 1, **HEC190K0.88**, **HEC230K1.05**, **HEC300K1.22**, **AEC160K0.44**, and **AEC200K0.64** are soluble in water only at low temperature, and the aqueous solution becomes turbid with increasing temperature. The temperature dependence of the optical transmittance for **HEC190K0.88** in water at the indicated c is shown in Fig. 4(A). The cloud point temperature T_{cloud} was estimated from the temperature at which the transmittance decreases to 90 % of the initial temperature. The resulting T_{cloud} data are plotted against c in Fig. 4(B). The cloud point temperature of the corresponding linear polymer tends to decrease with increasing DS and molar mass as illustrated in Fig. S10. Since the ethylcarbamate groups are hydrophobic in nature, the expansion of this biphasic region with increasing DS and molar mass is consistent with most polymer-poor solvent systems. This result might recall that the two-phase region of a branched polymer-solvent system is generally narrower than the corresponding linear chain as depicted in the Introduction (Alessi et al., 2004; Cowie et al., 1979; Sato et al., 1985; Tasaka et al., 2008; Terao et al., 1998; Yokoyama et al., 1991). However, the T_{cloud} for the highly branched chains is not very different from that for the linear chain with similar DS and n_w (Fig. 4(B)). In general, the solubility in water for the LCST systems is strongly related to the hydration and dehydration behavior with raising temperature. Considering the higher hydrophobic environment around ANS in HEC than in AEC as shown in Fig. 3, we can insist that intermolecular interactions between polymer chains and solvent molecules are inhibited by the bent helical

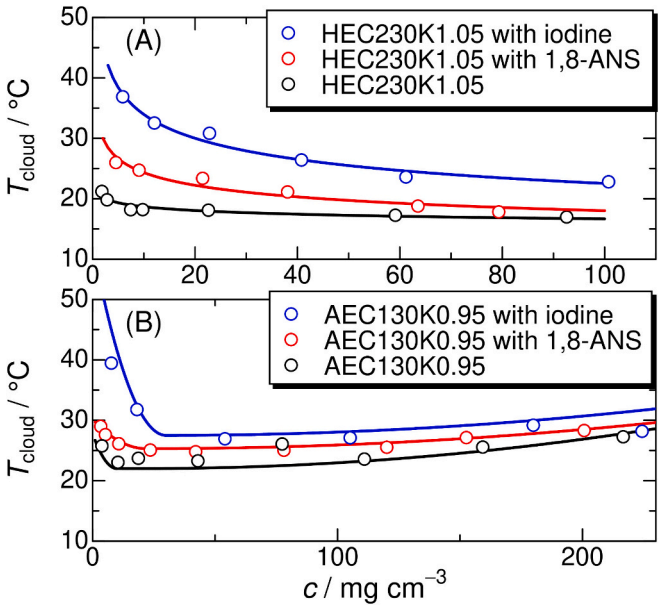

Fig. 5. Cloud point curves for (A) **HEC230K1.05** and (B) **AEC130K0.95** (filled circles) in water with indicated additives. $[I_2] = 1$ mM, [ANS] = 0.34 mM.

structure around the branching points. Consequently, we can conclude that the current highly branched polysaccharide samples tend to dehydrate and destabilize the one-phase solution compared to the linear chains. Similar behavior was also found for a branched polysaccharide derivative in an organic solvent, i.e., fully substituted HBCD in methyl acetate (Mizuguchi et al., 2023).

Complex formation with small molecules can affect the phase diagram. This has been observed for linear amylose carbamate derivatives (Kimura et al., 2020; Nakata et al., 2024) and polymeric crown ethers (Huang et al., 2018). Cloud point curves for **HEC230K1.05** and **AEC130K0.95** with or without small molecules are shown in Fig. 5. The concentration of small molecules was set to a constant $[I_2] = 1$ mM or [ANS] = 0.34 mM, independent of the polymer concentration c. T_{cloud} with small molecules is appreciably higher than without small molecules. Since iodine forms a complex with polysaccharide in the form of I_3^- or I_5^- and ANS has an anionic group in water, the difference in T_{cloud} is mainly due to electrostatic repulsion. This is reasonable because the difference becomes more significant with decreasing c. A more significant difference for highly branched chains may be related to the densely charged groups in the complex. However, we do not pursue this discussion further because there is no relevant thermodynamic theory for the phase diagram of polymer-solvent systems that properly accounts for

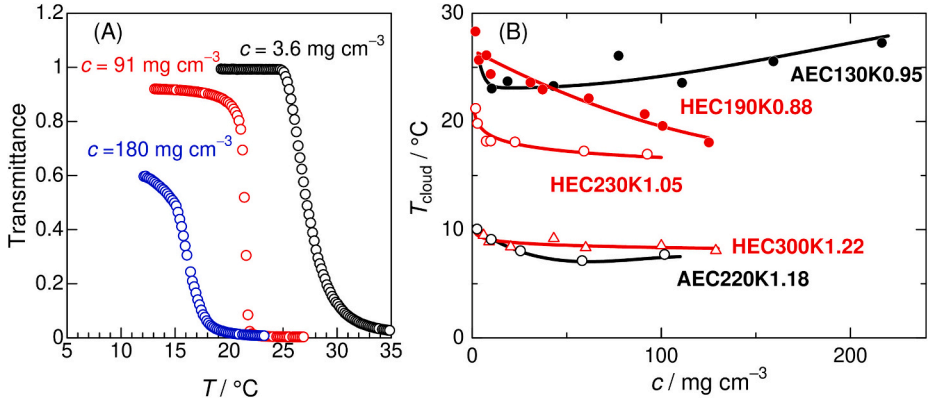

Fig. 4. (A) Temperature dependence of the optical transmittance for **HEC190K0.88** in water. $r_T = 1$ K/min. (B) Phase diagrams, cloud point temperature T_{cloud} vs the mass concentration c, for the indicated HEC highly branched) and AEC (linear) samples in water.

the branching effect.

4. Conclusions

The molecular shape of partially substituted highly branched cyclic dextrin ethyl carbamate behaves as a typical hyperbranched chain (HEC) in solution. The compact conformation was confirmed by small-angle X-ray scattering and viscosity measurements. Complex formation with iodine, 1-anilinonaphthalene-8-sulfonic acid (ANS), and pyrene was detected by appropriate spectroscopy. The results revealed that HEC has more hydrophobic environments inside the molecule while the helical structure induced by iodine is shorter than the linear chain due to the short partial chains and high segment density. Phase separation behavior was observed for the aqueous solution. The cloud point temperatures are almost the same as for the linear chains, while a much wider biphasic region is reported for the other branched polymers. This is most likely due to the fact that the branched structure and the hydration difference compensate each other.

CRediT authorship contribution statement

Akihito Kobayashi: Writing – original draft, Investigation, Formal analysis, Data curation. **Ken Terao:** Writing – review & editing, Writing – original draft, Supervision, Conceptualization.

Declaration of competing interest

The authors declare the following financial interests/personal relationships which may be considered as potential competing interests: Ken Terao reports financial support was provided by Japan Society for the Promotion of Science. If there are other authors, they declare that they have no known competing financial interests or personal relationships that could have appeared to influence the work reported in this paper.

Data availability

Data will be made available on request.

Acknowledgments

The authors are grateful to Dr. Noboru Ohta (SPring-8) for the SAXS measurements. The synchrotron radiation experiments were performed at the BL40B2 in SPring-8 with the approval of the Japan Synchrotron Radiation Research Institute (JASRI) (proposal Nos. 2019B1113, 2020A1132, 2020A0529, and 2021B1139). This work was the result of the use of research equipment (NMR and ultimate analysis) shared under the MEXT Project for promoting public utilization of advanced research infrastructure (Program for supporting construction of core facilities) Grant No. JPMXS0441200020 and JPMXS0441200021. This work was partially supported by JSPS KAKENHI grant Nos. JP20H02788 and JP23H02011.

Appendix A. Supplementary data

Additional figures for chemical reaction formula, ^{1}H NMR, ^{13}C NMR, FT-IR, SLS, SEC-MALS, UV-VIS absorption spectra, fluorescence spectra, and phase diagram including small molecules in water. Supplementary data to this article can be found online at doi: https://doi.org/10.1016/j.carbpol.2024.122473.

References

Alessi, M. L., Bittner, K. C., & Greer, S. C. (2004). Eight-arm star polystyrene in methylcyclohexane: Cloud-point curves, critical lines, and coexisting densities and viscosities. *Journal of Polymer Science Part B-Polymer Physics, 42*, 129–145. https://doi.org/10.1002/polb.10718

Asano, N., Kitamura, S., & Terao, K. (2013). Local conformation and intermolecular interaction of rigid ring polymers are not always the same as the linear analogue: Cyclic amylose tris(phenylcarbamate) in Theta solvents. *Journal of Physical Chemistry B, 117*, 9576–9583. https://doi.org/10.1021/jp406607w

Bizmark, N., Caggiano, N. J., Liu, J. X., Arnold, C. B., Prud'homme, R. K., Datta, S. S., & Priestley, R. D. (2022). Hysteresis in the thermally induced phase transition of cellulose ethers. *Soft Matter, 18*, 6254–6263. https://doi.org/10.1039/d2sm00564f

Browarzik, D., Langenbach, K., Enders, S., & Browarzik, C. (2013). Modeling of the branching influence on liquid-liquid equilibrium of binary and ternary polymer solutions by lattice-cluster theory. *Journal of Chemical Thermodynamics, 62*, 56–63. https://doi.org/10.1016/j.jct.2013.02.018

Burchard, W. (1969). Thermodynamic solution properties of 3 polymers exhibiting lower critical solution temperature. *Polymer, 10*, 467–475. https://doi.org/10.1016/0032-3861(69)90055-X

Burchard, W. (2004). Angular dependence of scattered light from hyperbranched structures in a good solvent. *A fractal approach. Macromolecules, 37*, 3841–3849. https://doi.org/10.1021/ma049950l

Chen, C., Zhang, W., Zhang, Y., Wang, P., & Ren, F. (2022). Tunable Thermo-responsive properties of Hydroxybutyl chitosan oligosaccharide. *Frontiers in Chemistry, 10*, Article 830516. https://doi.org/10.3389/fchem.2022.830516

Chevillard, C., & Axelos, M. A. V. (1997). Phase separation of aqueous solution of methylcellulose. *Colloid and Polymer Science, 275*, 537–545. https://doi.org/10.1007/s003960050116

Cowie, J. M. G., Horta, A., Mcewen, I. J., & Prochazka, K. (1979). Upper and lower critical solution temperatures for star branched polystyrene in cyclohexane. *Polymer Bulletin, 1*, 329–335. https://doi.org/10.1007/Bf01045420

Gericke, M., Atmani, Z., Skodda, L. H., & Heinze, T. (2024). Synthesis and characterization of polysaccharide carbamates and mixed carbamates with tunable water solubility. *Carbohydrate Polymer Technologies and Applications, 7*, Article 100479. https://doi.org/10.1016/j.carpta.2024.100479

Heymann, E. (1935). Studies on sol-gel transformations. I. The inverse sol-gel transformation of methylcellulose in water. *Transactions of the Faraday Society, 31*, 0846–0863. https://doi.org/10.1039/Tf9353100846

Huang, D. C., Zhang, Q., Deng, Y., Luo, Z., Li, B., Shen, X., … Chen, W. (2018). Polymeric crown ethers: LCST behavior in water and stimuli-responsiveness. *Polymer Chemistry, 9*, 2574–2579. https://doi.org/10.1039/c8py00412a

Jong, K., & Ju, B. Z. (2017). Thermo-responsive behavior of propynyl-containing hydroxyethyl starch. *Colloid and Polymer Science, 295*, 307–315. https://doi.org/10.1007/s00396-016-4009-1

Ju, B., Cao, S., & Zhang, S. (2013). Effect of additives on the cloud point temperature of 2-hydroxy-3-isopropoxypropyl starch solutions. *Journal of Physical Chemistry B, 117*, 11830–11835. https://doi.org/10.1021/jp404083r

Ju, B., Yan, D., & Zhang, S. (2012). Micelles self-assembled from thermoresponsive 2-hydroxy-3-butoxypropyl starches for drug delivery. *Carbohydrate Polymers, 87*, 1404–1409. https://doi.org/10.1016/j.carbpol.2011.09.028

Jung, Y., Kim, J. H., & Jang, W. D. (2017). Linear and cyclic poly(2-isopropyl-2-oxazoline)s for fine control of thermoresponsiveness. *European Polymer Journal, 88*, 605–612. https://doi.org/10.1016/j.eurpolymj.2016.09.003

Kimura, S., Kochi, R., Kitamura, S., & Terao, K. (2020). A temperature responsive polysaccharide derivative in aqueous solution: Amylose ethyl carbamates. *ACS Applied Polymer Materials, 2*, 2426–2433. https://doi.org/10.1021/acsapm.0c00366

Kishimoto, A., Mizuguchi, M., Ryoki, A., & Terao, K. (2022). Molecular structure and chiral recognition ability of highly branched cyclic dextrin carbamate derivative. *Carbohydrate Polymers, 290*, Article 119491. https://doi.org/10.1016/j.carbpol.2022.119491

Kishimoto, A., Ryoki, A., Kitamura, S., & Terao, K. (2023). Correlation between conformational feature in solution and chiral separation ability of linear and nonlinear amylose tris(alkylcarbamate)s. *Polymer, 284*, Article 126303. https://doi.org/10.1016/j.polymer.2023.126303

Klymchenko, A. S., & Mely, Y. (2013). Chapter two - fluorescent environment-sensitive dyes as reporters of biomolecular interactions. In M. C. Morris (Ed.), *Progress in molecular biology and translational science* (pp. 35–58). Academic Press. https://doi.org/10.1016/B978-0-12-386932-6.00002-8.

Knutson, C. A., Cluskey, J. E., & Dintzis, F. R. (1982). Properties of amylose-iodine complexes prepared in the presence of excess iodine. *Carbohydrate Research, 101*, 117–128. https://doi.org/10.1016/S0008-6215(00)80800-9

Kojima, H., Imamura, Y., Lu, Y. T., Yamago, S., & Koga, T. (2022). Experimental and theoretical studies on the phase behavior of aqueous solutions of structurally controlled Hyperbranched poly(N-isopropylacrylamide)s. *Macromolecules, 55*, 7932–7944. https://doi.org/10.1021/acs.macromol.2c01162

Lederer, A., & Burchard, W. (2015). Hyperbranched polymers: Macromolecules in between deterministic linear chains and dendrimer structures *(Polymer Chemistry Series Vol.* Vol. 16): Royal Society of Chemistry. doi:https://doi.org/10.1039/9781782622468.

McAllister, J. W., Schmidt, P. W., Dorfman, K. D., Lodge, T. P., & Bates, F. S. (2015). Thermodynamics of aqueous methylcellulose solutions. *Macromolecules, 48*, 7205–7215. https://doi.org/10.1021/acs.macromol.5b01544

Mizuguchi, M., Umeda, K., Mizumoto, H., & Terao, K. (2023). Solution characterization of a hyperbranched polysaccharide carbamate derivative and specific phase separation behavior due to chain branching. *Soft Matter, 19*, 7781–7786. https://doi.org/10.1039/d3sm01074k

Nakata, Y., Kitamura, S., & Terao, K. (2024). Dual thermoresponsive polysaccharide derivative – Water system. Partially substituted amylose butylcarbamate in water. *Carbohydrate Polymers, 325*, Article 121587. https://doi.org/10.1016/j.carbpol.2023.121587

Nilsson, G. S., Gorton, L., Bergquist, K.-E., & Nilsson, U. (1996). Determination of the degree of branching in Normal and amylopectin type potato starch with1H-NMR spectroscopy improved resolution and two-dimensional spectroscopy. *Starch, 48*, 352–357. https://doi.org/10.1002/star.19960481003

Nishida, K., Morita, H., Katayama, Y., Inoue, R., Kanaya, T., Sadakane, K., & Seto, H. (2017). Salting-out and salting-in effects of amphiphilic salt on cloud point of aqueous methylcellulose. *Process Biochemistry, 59*, 52–57. https://doi.org/10.1016/j.procbio.2016.12.009

Otto, S., Marina, P. F., Zhou, F., & Blencowe, A. (2021). Thermoresponsive polysaccharides with tunable thermoresponsive properties via functionalisation with alkylamide groups. *Carbohydrate Polymers, 254*, Article 117280. https://doi.org/10.1016/j.carbpol.2020.117280

Qiu, X.-P., Tanaka, F., & Winnik, F. M. (2007). Temperature-induced phase transition of well-defined cyclic poly(N-isopropylacrylamide)s in aqueous solution. *Macromolecules, 40*, 7069–7071. https://doi.org/10.1021/ma071359b

Ryoki, A., Kimura, Y., Kitamura, S., Maeda, K., & Terao, K. (2019). Does local chain conformation affect the chiral recognition ability of an amylose derivative? Comparison between linear and cyclic amylose tris(3,5-dimethylphenylcarbamate). *Journal of Chromatography A, 1599*, 144–151. https://doi.org/10.1016/j.chroma.2019.04.019

Sarkar, N. (1979). Thermal gelation properties of methyl and Hydroxypropyl methylcellulose. *Journal of Applied Polymer Science, 24*, 1073–1087. https://doi.org/10.1002/app.1979.070240420

Sato, S., Okada, M., & Nose, T. (1985). Critical solution point and chain dimension of branched-polystyrene solutions. *Polymer Bulletin, 13*, 277–284. https://doi.org/10.1007/bf00254663

Sato, T., Yang, J., & Terao, K. (2022). Micellar structure of hydrophobically modified polysaccharides in aqueous solution. *Polymer Journal, 54*, 403–412. https://doi.org/10.1038/s41428-021-00561-4

Takata, H., Ohdan, K., Takaha, T., Kuriki, T., & Okada, S. (2003). Properties of branching enzyme from Hyperthermophilic bacterium, Aquifex aeolicus, and its potential for production of highly-branched cyclic dextrin. *Journal of Applied Glycoscience, 50*, 15–20. https://doi.org/10.5458/jag.50.15

Takata, H., Takaha, T., Okada, S., Hizukuri, S., Takagi, M., & Imanaka, T. (1996). Structure of the cyclic glucan produced from amylopectin by Bacillus stearothermophilus branching enzyme. *Carbohydrate Research, 295*, 91–101. https://doi.org/10.1016/s0008-6215(96)90126-3

Tasaka, Y., Okumoto, M., Nakamura, Y., & Norisuye, T. (2008). Light scattering and phase separation studies on cyclohexane solutions of six-arm star polystyrene. *Polymer Journal, 40*, 634–639. https://doi.org/10.1295/polymj.PJ2008017

Terao, K., Okumoto, M., Nakamura, Y., Norisuye, T., & Teramoto, A. (1998). Light-scattering and phase-separation studies on cyclohexane solutions of four-arm star polystyrene. *Macromolecules, 31*, 6885–6890. https://doi.org/10.1021/ma980839n

Yang, J. Y., Peng, C. J., Liu, H. L., Hu, Y., & Jiang, J. W. (2006). A generic molecular thermodynamic model for linear and branched polymer solutions in a lattice. *Fluid Phase Equilibria, 244*, 188–192. https://doi.org/10.1016/j.fluid.2006.04.012

Yokoyama, H., Takano, A., Okada, M., & Nose, T. (1991). Phase-diagram of star-shaped polystyrene cyclohexane system - location of critical-point and profile of coexistence curve. *Polymer, 32*, 3218–3224. https://doi.org/10.1016/0032-3861(91)90145-9

Yuan, X., Ju, B., & Zhang, S. (2014). Novel pH- and temperature-responsive polymer: Tertiary amine starch ether. *Carbohydrate Polymers, 114*, 530–536. https://doi.org/10.1016/j.carbpol.2014.08.043

Zheng, B., Karski, M., & Taylor, S. D. (2019). Thermoresponsive hydroxybutylated starch nanoparticles. *Carbohydrate Polymers, 209*, 145–151. https://doi.org/10.1016/j.carbpol.2019.01.021